Energy-dispersive X-ray diffraction using an annular beam

A. J. Dicken,[1] J. P. O. Evans,[1,*] K. D. Rogers,[2] C. Greenwood,[2] S. X. Godber,[3] D. Prokopiou,[3] N. Stone,[4] J. G. Clement,[5] I. Lyburn,[6] R. M. Martin,[7] and P. Zioupos[2]

[1]Imaging Science Group, Rosalind Franklin Building, Nottingham Trent University, Nottingham, UK
[2]Cranfield Forensic Institute, Cranfield University, Shrivenham, UK
[3]Halo X-ray Technologies, Nottingham Trent University, Nottingham, UK
[4]Physics and Astronomy, University of Exeter, Exeter, UK
[5] University of Melbourne, Melbourne, Australia
[6]Cobalt Health, Cheltenham, UK
[7]Social and Community Medicine, University of Bristol, Bristol, UK
[*]paul.evans@ntu.ac.uk

Abstract: We demonstrate material phase identification by measuring polychromatic diffraction spots from samples at least 20 mm in diameter and up to 10 mm thick with an energy resolving point detector. Within our method an annular X-ray beam in the form of a conical shell is incident with its symmetry axis normal to an extended polycrystalline sample. The detector is configured to receive diffracted flux transmitted through the sample and is positioned on the symmetry axis of the annular beam. We present the experiment data from a range of different materials and demonstrate the acquisition of useful data with sub-second collection times of 0.5 s; equating to 0.15 mAs. Our technique should be highly relevant in fields that demand rapid analytical methods such as medicine, security screening and non-destructive testing.

OCIS codes: (050.1940) Diffraction; (340.0340) X-ray optics; (120.5820) Scattering measurements; (300.6560) Spectroscopy, x-ray.

References and Links

1. S. Pani, E. J. Cook, J. A. Horrocks, J. L. Jones, and R. D. Speller, "Characterization of breast tissue using energy-dispersive X-ray diffraction computed tomography," Appl. Radiat. Isot. **68**(10), 1980–1987 (2010).
2. G. Harding, H. Fleckenstein, D. Kosciesza, S. Olesinski, H. Strecker, T. Theedt, and G. Zienert, "X-ray diffraction imaging with the multiple inverse fan beam topology: principles, performance and potential for security screening," Appl. Radiat. Isot. **70**(7), 1228–1237 (2012).
3. G. Harding, "X-ray diffraction imaging-a multi-generational perspective," Appl. Radiat. Isot. **67**(2), 287–295 (2009).
4. O. Lazzari, S. Jacques, T. Sochi, and P. Barnes, "Reconstructive colour X-ray diffraction imaging-a novel TEDDI imaging method," Analyst (Lond.) **134**(9), 1802–1807 (2009).
5. A. M. Beale, S. D. M. Jacques, E. K. Gibson, and M. Di Michiel, "Progress towards five dimensional diffraction imaging of functional materials under process conditions," Coord. Chem. Rev. **277–278**, 208–223 (2014).
6. E. J. Cook, J. A. Griffiths, M. Koutalonis, C. Gent, S. Pani, J. A. Horrocks, L. George, S. Hardwick, and R. Speller, "Illicit drug detection using energy dispersive X-ray diffraction," in Proceedings of SPIE, Non-Intrusive Inspection Technologies II, 73100I (2009).
7. D. O'Flynn, C. B. Reid, C. Christodoulou, M. D. Wilson, M. C. Veale, P. Seller, D. Hills, H. Desai, B. Wong, and R. Speller, "Explosive detection using pixellated X-ray diffraction (PixD)," J. Instrum. **8**(3), P03007 (2013).
8. K. Wells and D. A. Bradley, "A review of X-ray explosives detection techniques for checked baggage," Appl. Radiat. Isot. **70**(8), 1729–1746 (2012).
9. K. Rogers, P. Evans, J. Rogers, J. Chan, and A. Dicken, "Focal construct geometry – a novel approach to the acquisition of diffraction data," J. Appl. Cryst. **43**(2), 264–268 (2010).
10. P. Evans, K. Rogers, J. Chan, J. Rogers, and A. Dicken, "High intensity x-ray diffraction in transmission mode employing an analog of Poisson's spot," Appl. Phys. Lett. **97**(20), 204101 (2010).
11. A. Dicken, A. Shevchuk, K. Rogers, S. Godber, and P. Evans, "High energy transmission annular beam X-ray diffraction," Opt. Express **23**(5), 6304–6312 (2015).

12. D. Prokopiou, K. Rogers, P. Evans, S. Godber, and A. Dicken, "Discrimination of liquids by a focal construct X-ray diffraction geometry," Appl. Radiat. Isot. **77**, 160–165 (2013).
13. P. Evans, K. Rogers, A. Dicken, S. Godber, and D. Prokopiou, "X-ray diffraction tomography employing an annular beam," Opt. Express **22**(10), 11930–11944 (2014).
14. R. D. Luggar, J. A. Horrocks, R. D. Speller, and R. J. Lacey, "Determination of the geometric blurring of an energy dispersive X-ray diffraction (EDXRD) system and its use in the simulation of experimentally derived diffraction profiles," Nucl. Instrum. Methods Phys. Res., Sect. A **383**(2-3), 610–618 (1996).
15. B. Ghammraoui, V. Rebuffel, J. Tabary, C. Paulus, L. Verger, and P. Duvauchelle, "Effect of grain size on stability of X-ray diffraction patterns used for threat detection," Nucl. Instrum. Methods Phys. Res., Sect. A **683**, 1–7 (2012).

1. Introduction

There is a growing need for rapid in situ materials discrimination in fields including medicine [1], security screening [2,3] and industrial process control [4]. X-ray diffraction (XRD) is the gold standard for conducting definitive materials discrimination because it provides the near unequivocal identification of material phase. Constructive interference of X-rays occurs when Bragg's condition, $n\lambda = 2d\sin\theta$ is satisfied. Where λ is the wavelength of radiation, d the inter-planar spacing, 2θ the diffraction angle through which coherent X-rays are scattered and n is a positive integer specifying the order of diffraction. If a sufficient subset of the d-spacings present in a material can be derived then material phase identification is made possible. In principle, this may be accomplished by one of two, contrasting, X-ray diffraction methods; namely angular-dispersive X-ray diffraction (ADXRD) and energy-dispersive X-ray diffraction (EDXRD). Traditional laboratory based diffractometers employ the ADXRD approach. The sample is interrogated by a monochromatic beam of radiation and the angle, 2θ, of the resultant diffracted X-rays is measured to enable the associated d-spacing's to be calculated. The advent of modern 2D detectors negates the need for moving components [5], yet this approach is still renowned for its high specificity rather than speed [6]. It does not provide an effective basis for the development of high-speed applications. Alternately, EDXRD employs a polychromatic source to measure the energy of the diffracted X-rays (or in effect λ according to Planck's energy-frequency relation) at a fixed angle of scattering. However, while EDXRD is favored for rapid analysis, the increase in flux afforded by the broadband spectrum is limited by the need for high aspect ratio collimators i.e. collimators with a low angular acceptance, which limits the total amount of diffracted flux incident upon the detector [7]. This consideration is compounded by the relatively low values of coherent scatter cross section e.g. typically <1% of the incident primary beam is coherently scattered. Therefore, time critical applications based upon XRD are inherently problematic [8]. An alternate ADXRD technique termed focal construct geometry (FCT) has previously been shown to increase the measured diffraction intensities by ~20 times using commercial off the shelf (COTS) low cost components [9,10]. We have recently been able to adapt this technique to work in an energy-dispersive capacity by employing a stationary energy resolving point detector. In this paper we present the first FCT energy-dispersive diffractograms measured from a range of different materials and demonstrate sub-second data collection times.

2. Methods

2.1 Theory background

The theory of focal construct technology (FCT) has been discussed in detail elsewhere [9,10]. To summarize FCT is an alternate ADXRD geometry that employs an annular beam of monochromatic radiation. When this beam is incident normally upon a semi or polycrystalline material Debye cones are generated within an annular gauge volume. A continuum of Debye cones is produced, according to Bragg's condition, for each d-spacing at characteristic angles, 2θ. Providing that 2θ is greater than the annular beam opening angle then each "2θ family" of Debye cones forms a high intensity monochromatic focal spot along the symmetry axis. All prior work with FCT has employed irradiance measurements using either quasi-

monochromatic or pseudo-monochromatic X-rays as the basis for an angular dispersive method. These techniques detect the presence of Bragg maxima in the form of focal spots by either translating the detector [9,10] (with a fixed sample/source configuration) or translating the sample [11] (with a fixed detector/source position) along the principal axis. Thereby enabling the diffraction angle, 2θ, to be measured and the corresponding d-spacings to be calculated using the known geometric relationship between the source, sample and detector. FCT has been shown to deal favorably with non-ideal samples such as those exhibiting large grain size, preferred orientation and liquid samples [12] that exhibit only short-range order. In addition, ADXRD tomography employing an annular beam has been demonstrated [13] as well as high energy versions (W-Kα) that employ balance filtering [11].

2.2 New energy-dispersive FCT approach

In contrast to previous FCT methods we employ a stationary energy resolving "point" detector to measure a polychromatic focal spot comprised of diffracted X-rays from a sample. The broad incident spectrum of the annular beam increases the intensity of the diffracted flux incident upon the detector and facilitates relatively high-speed operation. In common with most EDXRD implementations our new technique negates the need for moving the detector or the sample during signal acquisition. Therefore, the novelty of our ED FCT lies within the geometry employed to produce the polychromatic focal spots.

It can be appreciated from Bragg's condition that polychromatic diffracted flux from an annular gauge volume (for a single d-spacing) can produce a focal spot extended in spectral energy and distributed along the Z-axis, as depicted in Fig. 1.
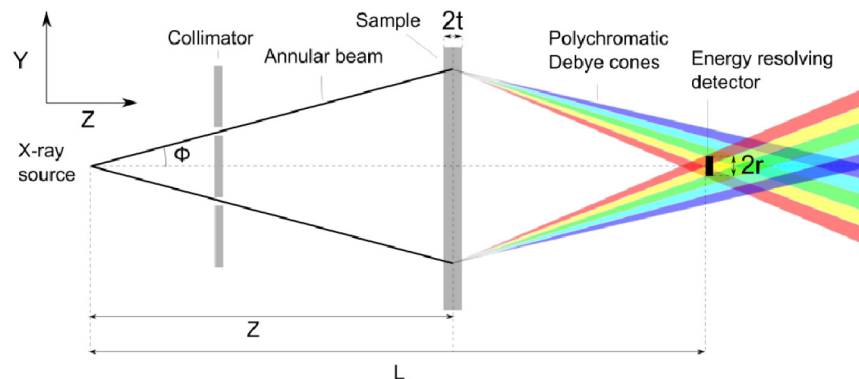

Fig. 1. Schematic showing an annular beam incident normally upon an extended polycrystalline sample. The diffracted flux from the annular gauge volume, for a single d-spacing, is spread over a range of different X-ray energies (higher energy flux is represented in blue while the lower energy flux is represented in red). An energy resolving point detector is used to sample the resultant polychromatic focal spot.

It can also be appreciated from Fig. 1 that as the wavelength of the coherent scatter reduces so too does 2θ. It follows that a focal spot exhibiting a narrow spectral range can be measured by a finite detector at some position along the linear extension of the polychromatic focal spot. Through similar reasoning it can be appreciated that when a number of different d-spacings satisfy Bragg's condition then in effect a series of "monochromatic" spots can be incident simultaneously upon a stationary point detector. This scenario is illustrated in Fig. 2, where two-dimensional diffraction patterns arising from relatively small, intermediary and large d-spacings form spatially superimposed but spectrally discrete diffraction spots.
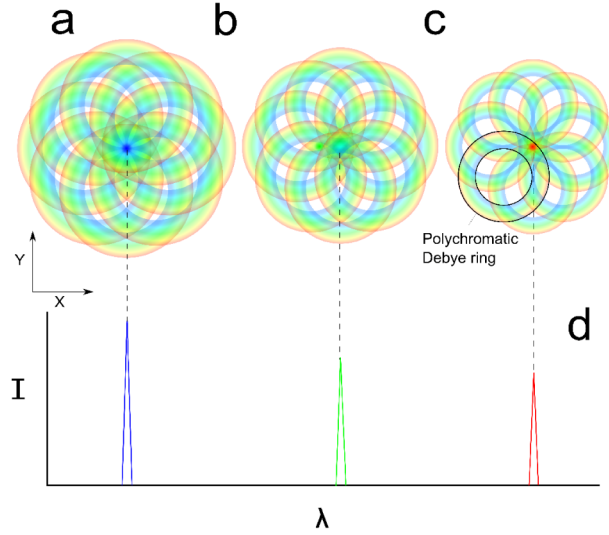
Fig. 2. Discretized representation of a continuum of polychromatic Debye rings produced by FCT for relatively small (a), intermediary (b), and large (c) d-spacing. These patterns occur in the detection plane normal to the annular beam symmetry axis and in practice are superimposed upon each other. At the center of each composite pattern is a high intensity focal spot (Bragg maxima), which may be sampled with an energy resolving point detector to produce an intensity against wavelength plot (d). Note that we employ the term *polychromatic Debye ring* to describe the spread in spectral energy (and annular width) for a single d-spacing over a finite spread in diffraction angle, $\Delta 2\theta$. However, the ring component of each polychromatic Debye ring that contributes to the intensity of an incident focal spot has a fixed radius (e.g. approximately 32 mm for the FCT/sample configuration employed in our experiments).

The following analysis assumes that an annular primary X-ray beam in the form of a conical shell is incident with its symmetry axis normal to a flat sample of finite thickness.

To derive an appropriate relationship between d-spacings and spectral measurements we consider the diffracted beam from an annular gauge volume, which subtends a sample of half-thickness, t, at a source-to-sample distance, Z. The uncollimated diffracted flux is sampled by a detector of radius, r, at distance, L from the X-ray point source. The finite size of the X-ray source is considered negligible. The resultant angular distribution of the diffracted beam is bounded by a maximum, $2\theta_{max}$, and a minimum, $2\theta_{min}$, value according to

$$2\theta_{max} = \tan^{-1}\left[\frac{(Z+t)\tan\phi_{max}+r}{L-Z-t}\right]+\phi_{max}. \tag{1}$$

$$2\theta_{min} = \tan^{-1}\left[\frac{(Z-t)\tan\phi_{min}-r}{L-Z+t}\right]+\phi_{min}. \tag{2}$$

Where ϕ_{max} and ϕ_{min} are the maximum and minimum half-opening angles of the primary beam envelope, respectively. Therefore, the angular spread of the primary beam about a mean angle ϕ is given by, $\Delta\phi = \phi_{max} - \phi_{min}$. A nominal 2θ value is obtained by setting; r=0, t=0 and, $\phi_{max} = \phi_{min} = \phi$, in either Eqs. (1) or (2) as the resultant equation is identical. Under these hypothetical conditions the angular distribution of the diffracted beam describes a surface of a tubular right cone with its base at the mean sample position Z, and its apex at the point detector position, L. Therefore, d-spacing is estimated by substituting for θ in Bragg's law, $n\lambda = 2d\sin\theta$ to give

$$d = \frac{n\lambda}{2\sin\left(\frac{1}{2}\left(\tan^{-1}\left[\frac{Z\tan\phi}{L-Z}\right] + \phi\right)\right)}. \tag{3}$$

However, the spread in diffraction angle, $\Delta 2\theta = 2\theta_{max} - 2\theta_{min}$ from consideration of Eqs. (1) and (2) enables a range of spectral energies (or wavelengths, λ) to satisfy Bragg's condition. Therefore, for a given d-spacing the first order spread in wavelength is bounded by maximum, λ_{max}, and minimum, λ_{min}, values given by

$$\lambda_{max,min} = 2d\sin\left(\frac{2\theta_{max,min}}{2}\right). \tag{4}$$

In practice the measurement of the spectral width described by Eq. (4) will also be subject to the energy resolution of the detector, ΔE at full width at half-maximum (FWHM). The energy resolution of the detector may be expressed as a wavelength following $\lambda_D = hc/\Delta E$ and the resultant spread in wavelength, Δe_λ, is given by

$$\Delta e_\lambda = \left(\frac{\lambda_{max}\lambda_D}{\lambda_D - \lambda_{max}}\right) - \left(\frac{\lambda_{min}\lambda_D}{\lambda_D + \lambda_{min}}\right). \tag{5}$$

Equation (5) may also be expressed in terms of spectral energy; $E_{max,min} = hc/\lambda_{min,max}$ as $\Delta e_\lambda = hc\left\{\left[1/(E_{min}-\Delta E)\right] - \left[1/(E_{max}+\Delta E)\right]\right\}$ where h is the Planck constant and c is the speed of light.

The resultant spread in d-spacing, Δd, is given by

$$\Delta d = \frac{\Delta e_\lambda}{2\sin\theta}. \tag{6}$$

2.3 Experiment conditions

Our experiments were conducted using a Hamamatsu microfocus X-ray source with a tungsten target and a focal spot size of 40 μm; the accelerating voltage and current were 130 kV, 300 μA, respectively. An annular beam with an opening angle of 3.92° ± 0.05°; $\phi_{max} = 3.97^o$, $\phi_{min} = 3.87^\circ$ was produced with the aid of a bespoke tungsten optic. Scattered rays were detected using an Amptek CdTe X-ray spectrometer with a 9 mm^2 circular detector and typical FWHM of 850 eV. The detector was positioned centrally and normal to the symmetry axis of the annular beam at L = 460 mm. Integration times are reported in each figure respectively. Conventional 1d diffractograms were produced by taking energy measurements and calculating d-spacing using Eq. (3). Sample materials were placed at a mean position of Z = 138 mm from the X-ray source. This configuration provided a nominal 2θ angle of 5.6°. A Savitzky-Golay smoothing filter has been applied to each diffractogram using the function sgolayfilt in Matlab®. The origin of each reference standard is stated in Table 1.

Table 1. Material name, chemical formula, sample thickness, reference standard source and comments.

Material	Chemical formula	Sample thickness (mm)	ICDD pdf card numbers	Comments
calcite	$CaCO_3$	10	00-005-0586	
calcium hydroxide	$Ca(OH)_2$	10	00-004-0733	
stainless steel	$FeCr_{0.29}N_{0.16}C_{0.06}$	1	00-033-0397	
copper	Cu	1	00-001-1241	Preferred orientation
talcum powder	$H_2Mg_3(SiO_3)_4$	10	00-013-0558	
sodium chlorate	$NaClO_3$	10	01-675-1619	
cortical bone	-	10	Empirical (Sect. 2.3)	Bovine femur
hydroxyapatite	$Ca_{10}(PO_4)_6(OH)_2$	10	Empirical (Sect. 2.3)	
sucrose	$C_{12}H_{22}O_{11}$	10	00-001-0528	Caster sugar (large grain)
sucrose	$C_{12}H_{22}O_{11}$	10	00-001-0528	Icing sugar (small grain)

Where the reference standards have been obtained empirically the patterns were collected by a Bruker D8 diffractometer with a Cu target. All energy-dispersive FCT diffraction patterns have been background subtracted by employing an equivalent integration period but with no sample present.

3. Results and discussion

Energy-dispersive diffraction patterns from a number of different sample materials were collected using three different integration times; 10, 1 and 0.5 seconds; equating to 3, 0.3 and 0.15 mAs. The nominal diffraction angle, $2\theta = 5.6°$, was calculated by considering an infinitesimally small; primary beam width, sample thickness and detector size using Eq. (1) or identically, Eq. (2). Spectral energy measurements were converted into d-spacing following Eq. (3) as shown in Fig. 3. Each diffractogram has been time normalized so that they appear on equivalent scales. Also, examples of the spectral energy patterns obtained for several different materials are shown in Fig. 4. It can be appreciated that scattering intensity is linear with respect to the integration time. Some degradation can be seen with decreasing integration time although peak positions and relative intensities still exhibit good correspondence. Also, good correspondence between the FCT peak positions and the standard peak positions can be observed. However, the FCT peaks do exhibit significant broadening due to geometric broadening. This type of systematic broadening in transmission EDXRD measurements was anticipated and is well understood [14]. It can arise due to the concatenated effects of sample thickness, primary/diffraction beam collimation and detector size and finite energy resolution.
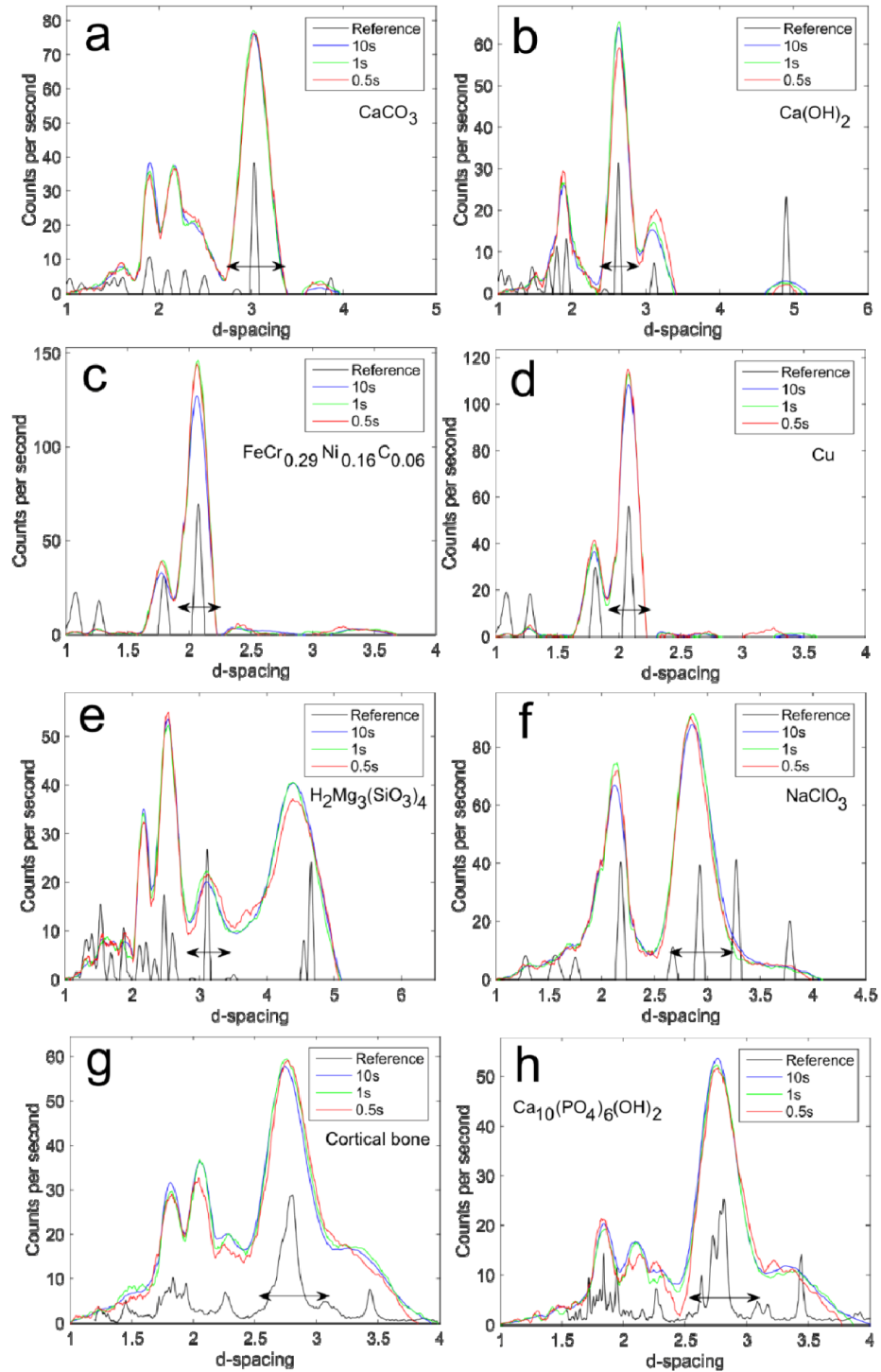
Fig. 3. X-ray diffraction patterns from various materials for 10, 1 and 0.5 seconds integration time, respectively. Counts per second have been time normalized with respect to the integration time. A Savitzky-Golay smoothing filter has been applied. The d-spacings are given in Å.
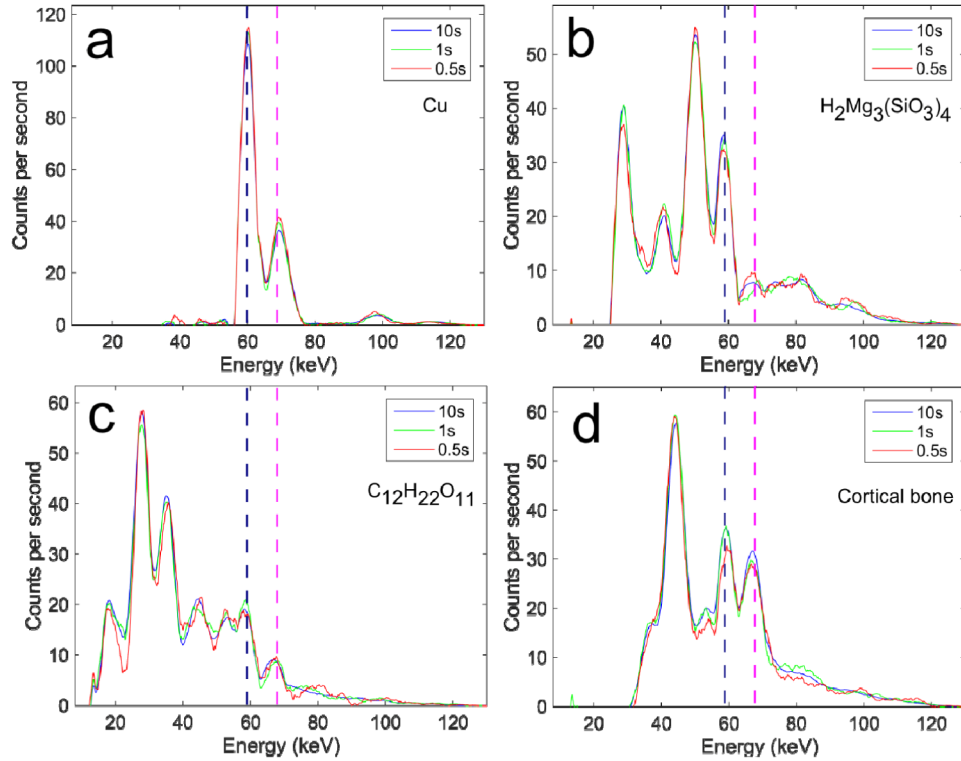
Fig. 4. X-ray diffraction patterns from various materials for 10, 1 and 0.5 seconds integration time, respectively. Counts per second have been time normalized with respect to the integration time. A Savitzky-Golay smoothing filter has been applied. The expected position of the W-Kα (≈58 keV) scattering line(s) and W-Kβ (≈67 keV) lines are indicated by vertical dotted lines, respectively.

The relative contributions to geometric broadening attributable to the physical parameters are quantified in different combinations using Eqs. (1) and (2), and tabulated in Table 2. The geometric broadening attributed to each parameter $r, t, \Delta\phi$ is; 65%, 18%, 15%, respectively (i.e. rows 4, 6 and 7 in Table 2). It can also be appreciated from Table 2 that there is an approximate twofold increase in geometric broadening attributable to the finite detector size (row 4) in comparison with the combination of primary beam divergence and sample half-thickness (row 5). The range of wavelengths, λ, that are able to satisfy Bragg's condition was calculated following Eq. (4). In this analysis the detector broadening was set to be zero i.e. ΔE = 0, and λ_D is considered to approach infinity, thus Eq. (5) reduces to, $\Delta e_\lambda = \lambda_{max} - \lambda_{min}$. The corresponding spread in d-spacing, following Eq. (6), attributed to the geometric parameters $r, t, \Delta\phi$ is shown in the graph of Fig. 5. The separations between corresponding linear plots (i.e. error envelopes) demonstrate that Δd increases linearly for increasing d-spacing.

To show the compounding effect of the detector energy resolution, 850 eV FWHM, the total calculated spectral broadening $\Delta e_\lambda = f(r, t, \Delta\phi, \Delta E)$ was concatenated into d-spacing and plotted as the outer "error envelope" in Fig. 5. It can be appreciated from this plot that Δd increases nonlinearly, as predicted by Eqs. (5) and (6). Therefore, the compounding of geometric blurring with detector broadening becomes increasingly significant for relatively large d-spacing values as evidenced in our experiment patterns.

Table 2. Calculated geometric broadening, $\Delta 2\theta$, is tabulated in terms of different combinations of the primary beam divergence, detector radius and sample half-thickness. Note that a table entry of 0 selects $\left(\phi_{max}=\phi_{min}=3.92^{\circ}, r=0, t=0\right)$, and a table entry of 1 selects $\left(\phi_{max}=3.97^{\circ}, \phi_{min}=3.87^{\circ}, r=1.7\,\text{mm}, t=5\,\text{mm}\right)$, respectively.

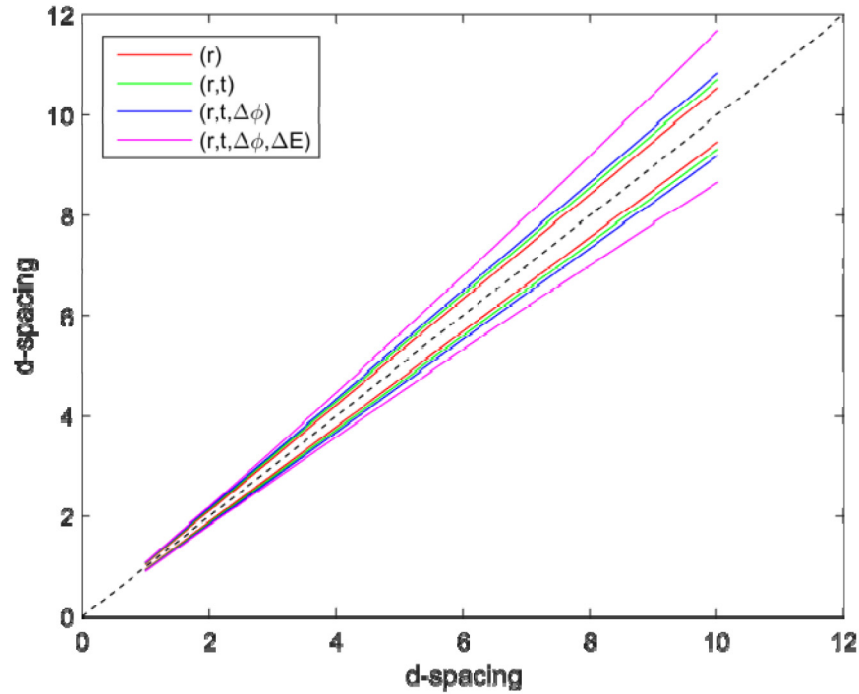|	Primary beam divergence $\phi_{max}=3.97^{o}$ $\phi_{max}=3.87^{\circ}$ $\phi=3.92^{\circ}$	Detector radius $r=1.7\,\text{mm}$	Sample half-thickness $t=5\,\text{mm}$	$\Delta 2\theta$ (degrees)
1	1	1	1	0.92
2	0	1	1	0.78
3	1	1	0	0.75
4	0	1	0	0.60
5	1	0	1	0.32
6	0	0	1	0.17
7	1	0	0	0.14

Fig. 5. Plots showing the calculated spread in d-spacing, Δd, in terms of the contributions from r = 1.7 mm in combination with; t = 5 mm, $\Delta\phi = 3.92^{\circ} \pm 0.05^{\circ}$, and ΔE = 850 eV . For example, the inner "error envelope" represents the contribution from the detector radius, r, alone, while the "outer error" envelope shows the compound effect of all the physical parameters $r, t, \Delta\phi, \Delta E$. The vertical separation between corresponding plots (that define each error envelope) indicates the associated Δd. The reference line (dotted) has a gradient of unity.

The relatively weak affect of the sample half-thickness upon peak broadening can be appreciated by comparing the patterns for the $t=0.5\,\text{mm}$ stainless steel and copper samples, see Figs. 3(c) and 3(d), with the $t=5\,\text{mm}$ samples i.e. all other samples. This observation was predicted by Eqs. (1) and (2), as $Z \gg t \ll (L-Z)$ e.g. $t:Z$ and $t:(L-Z)$ are approximately

1 : 28 and 1:64, respectively for t = 5 mm. Thus, a tenfold reduction in sample half-thickness has a relatively small impact upon peak width in our experiment patterns.

This analysis of has been found to be a useful indicator of first order peak spread and specific examples are highlighted by the horizontal bars about principal reference peaks on our experiment diffractograms shown Fig. 3 (Table 3 lists the corresponding Δd values). We have found that the FCT diffractograms are consistent with the spectral broadening and spread in d-spacing predicted by Eqs. (1)-(6). However, in the future we plan to conduct more detailed analysis by employing Monte Carlo ray-tracing as an effective way to account for all effects simultaneously beyond first order.

Table 3. Material name, true d-spacing, and calculated spread in d-spacing. The
Δd values are highlighted by the horizontal bars in the corresponding diffractograms in
Figs. 3 and 6.

Material	d-spacing (Å)	Δd (Å)
sucrose	3.5900	0.77
calcite	3.0350	0.62
calcium hydroxide	2.6280	0.53
talc	3.1160	0.64
sodium chlorate	2.9293	0.60
hydroxyapatite	2.8040	0.57
cortical bone	2.8040	0.57
stainless steel	2.0750	0.34
copper	2.0800	0.34

The contribution to spectral broadening attributed to $t, \Delta\phi$ is relatively small in comparison with the detector broadening, r, as previously discussed and highlighted in Fig. 5. Therefore, it is feasible to investigate whether the geometric effects can be made negligible relative to detector broadening. The most obvious way forward would be to restrict the solid angle subtended by the detector by employing high aspect ratio collimation of the diffracted flux. This method could be employed usefully in future work to reduce peak widths and improve potentially d-spacing resolution especially at the lower energy, longer wavelength, part of the spectrum i.e. for relatively large d-spacings.

In comparison to the reference standard peaks the corresponding FCT patterns appear reduced in intensity for relatively small d-spacings <1.4 Å i.e. those obtained via spectral energy measurements taken at >90 keV. This effect was attributed to the characteristic spectral shape of the 130 keV tungsten X-ray source, which for >90 keV produced a relatively low total number of photons. This effect was compounded by the reducing coherent scatter cross section for increasing X-ray energy. This trend is observed typically in EDXRD results obtained from X-rays generated using thermionic emission and can be improved, to some extent, by employing a higher energy (increased maximum keV) X-ray source. Conversely, an intensity perturbation is observed at ~2.15 Å, which can be attributed to the tungsten X-ray source Kα (≈58 keV) lines, see Figs. 3(a), 3(g), and 3(h), or as a shoulder on an existing peak, see Figs. 3(c), 3(d), and 3(f).

Large grain size has been shown to be problematic for EDXRD experiments [15]. Peak intensity is related to the number of illuminated grains in the correct orientation to satisfy Bragg's condition. A powder diffraction model assumes typically that crystallite orientations are randomly distributed such that each d-spacing is represented proportionally. However, particle size statistics concerning large grain size indicates that "super peaks" and/or the disappearance of peaks in EDXRD spectra are possible and can make material phase identification problematic. This important issue has been investigated previously [15] by measuring diffractograms from caster sugar and icing sugar as these materials share the same molecular structure i.e. both are sucrose but have different grain sizes (0.15 mm^3-0.65 mm^3 and ≈0.07 mm^3 grain volumes for caster and icing sugar, respectively). We conducted a similar experiment; see Fig. 6, but employed our FCT method. The resultant diffractograms

from the icing sugar and caster sugar samples are illustrated in Figs. 6(a) and (b), respectively.
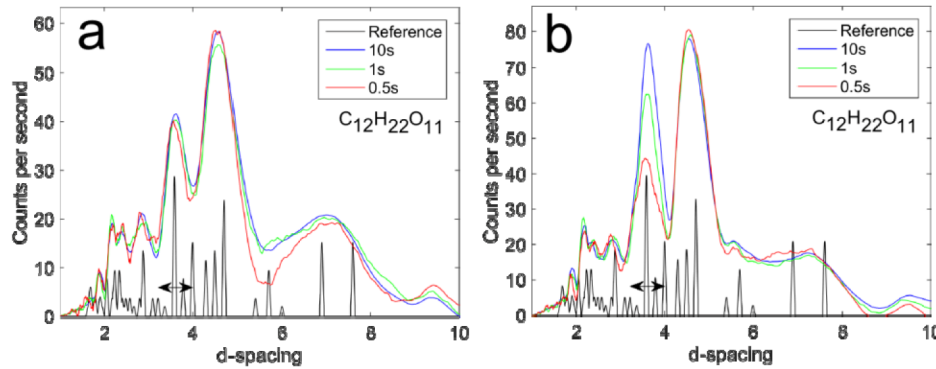

Fig. 6. X-ray diffraction patterns from small (a), and large (b) grained sucrose for 10, 1 and 0.5 second integration times, respectively. A Savitzky-Golay smoothing filter has been applied. The d-spacings are given in Å.

We noted little peak instability in our resultant diffractograms. Thus both the small and large grained sucrose could be reliably identified from the patterns in spite of some peak intensity fluctuations. This observation would seem logical since FCT is not subject to the focusing constraints encountered by EDXRD techniques employing a linear fan beam [15]. Therefore, a relatively increased total number of crystallites can contribute to the FCT patterns as consistent with our previous "monochromatic" implementations of FCT, which have also demonstrated reasonably stable measurements for samples exhibiting large grain size [9].

4. Conclusion

We show that material phase can be established by measuring the spectral profile of a polychromatic diffraction spot from an annular gauge volume. Unlike previous angular dispersive (monochromatic) FCT work there is no requirement to take multiple measurements along the principal axis of the annular beam to obtain structural information. Consequently, in common with most EDXRD methods our new approach does not require moving components, which is advantageous for many applications. We also demonstrate reliable phase identification by employing an uncollimated point detector. Our theoretical analysis indicated that the finite size of the detector was a major contributor to the geometric blurring evidenced via the peak broadening in the resultant diffractograms. The relative contribution to geometric broadening by the physical parameters; $r, t, \Delta\phi$ was 65%, 18%, 15%, respectively.

In the future we plan to investigate collimation of the diffracted flux to reduce peak widths. We have realized a significant decrease in the integration times i.e. 0.5 s; equating to 0.15 mAs by utilizing the polychromatic spectrum. The fidelity of our approach appeared robust in terms of peak position when the scattering distributions measured were adversely affected by large grain size (typically problematic for EDXRD configurations [15]). The stability in the FCT measurements was due to the relatively extended (annular) gauge volume providing enhanced particle size statistics.

It is hoped that this work will form the basis for a diagnostic tool for applications that require high fidelity materials characterization, are time critical, require in situ measurement and are cost sensitive. Fields that are likely to benefit from this technology include medicine, security screening and non-destructive testing.

Acknowledgments